Ultrafast Internal Conversion Dynamics of Highly Excited Pyrrole Studied with VUV/UV Pump Probe Spectroscopy

Spencer L. Horton[1], Yusong Liu[1], Pratip Chakraborty[2], Spiridoula Matsika[2], and Thomas Weinacht[1]
[1]*Department of Physics and Astronomy, Stony Brook University, Stony Brook, NY 11794, USA and*
[2]*Department of Chemistry, Temple University, Philadelphia, PA 19122, USA*

(Dated: 24 January 2017)

We study the relaxation dynamics of pyrrole after excitation with an 8 eV pump pulse to a state just 0.2 eV below the ionization potential using VUV/UV pump probe spectroscopy. Our measurements in conjunction with electronic structure calculations indicate that pyrrole undergoes rapid internal conversion to the ground state in less than 300 fs. We find that internal conversion to the ground state dominates over dissociation.

I. INTRODUCTION AND MOTIVATION

Pyrrole (C_4H_5N), has been of intense experimental[1–8] and theoretical interest[9–15] because it is considered an important building block for understanding the ultrafast dynamics of larger pyrrole-containing biomolecules, such as hemoglobin, vitamin B_{12}, chlorophyll, and tryptophan. Pyrrole exhibits rich photo-induced dynamics when excited with UV radiation. Internal conversion and dissociation have been studied extensively both experimentally and theoretically.

Experimental work on the relaxation dynamics of photoexcited pyrrole has focused on pumping the first absorption band, with time resolved studies probing the fate of molecules excited with pump wavelengths between 200 and 260 nm[2–7]. These experiments, which made use of ionization as a probe, established that the molecule undergoes rapid internal conversion and dissociation on timescales of $\sim$ 100 fs or less. Experiments that made use of velocity map imaging to measure the momentum of Hydrogen ions generated by the probe pulse[3] found both fast and slow H^+, indicating dissociation on both the excited and ground state surfaces. The relative yields indicated that dissociation on the excited state dominated over internal conversion to the ground state followed by dissociation.

Several theoretical studies have examined the excited state dynamics in pyrrole. Three pathways involving conical intersections between S_1 and S_0 have been identified which are involved in nonadiabatic decay to the ground state or dissociation.[9–15] In particular dissociation along the NH bond has been found to be important in many studies. Recent theoretical work by Barbatti *et al*[10] using the trajectory surface hopping approach with excitation energies between 193 nm and 248 nm indicated that while excitation to the first absorption band (wavelength of 248 nm) led to N-H bond stretching and fission, excitation with higher energy to the second absorption band (wavelength of 193 nm) led to slower decay (timescales of about 200 fs) with more complicated dynamics. In this work, we consider excitation of pyrrole with pulses in the vacuum ultraviolet (VUV), corresponding to an excitation energy of about 8 eV. This corresponds to a higher excitation energy than all previous experiments and is motivated by the question of how the initial excitation influences the relaxation dynamics. Of particular interest in this study is whether the decay of the excited state is primarily due to dissociation on an excited state surface, or internal conversion to the ground state. In previous work where we studied the relaxation dynamics of radical cations (uracil, 1-3 cyclohexadiene, and hexatriene) using trajectory surface hopping[16], we found that relaxation to the ground ionic state was rapid (<100 fs), taking place before dissociation. The density of states in these cations is similar to the density of states in highly excited pyrrole, and thus while excitation at lower energy resulted primarily in dissociation, we expect more competition between internal conversion and dissociation at higher energies.

We probe the excited state dynamics with a UV pulse having a $\sim$5 eV photon energy, which allows us to ionize from any excited state of the molecule without background signal from the ground state. We measure a decay time from this high-lying state of approximately 200 fs.

II. EXPERIMENTAL APPARATUS

We use a Ti:Sapphire laser (1.2 mJ, 1 kHz, 30 fs, 780 nm) to generate ultrafast UV and Vacuum-UV (VUV) pulses. In conjunction with a time-of-flight mass spectrometer (TOFMS), we make use of these pulses to perform pump-probe ion yield measurements on pyrrole. Gas-phase pyrrole molecules are injected into the vacuum chamber as an effusive molecular beam.

Our experimental setup can be seen in Fig.[1]. The IR beam from the amplifier is split into two portions which have pulse energies of 1.1 mJ and 100 μJ. The 1.1 mJ of IR is used to create 50 μJ of UV ($\hbar\omega$ = 4.78 eV) light through second-harmonic-generation (SHG) followed by third-harmonic-generation (THG) in BBO crystals with a calcite delay compensator. An uncoated 1 mm thick CaF_2 window is inserted into the beam at 45° to act as a beamsplitter for the UV. The 5 μJ pulse from the front surface reflection of the CaF_2 window is used as the UV probe in our experiments. Approximately 100 nJ of fifth-

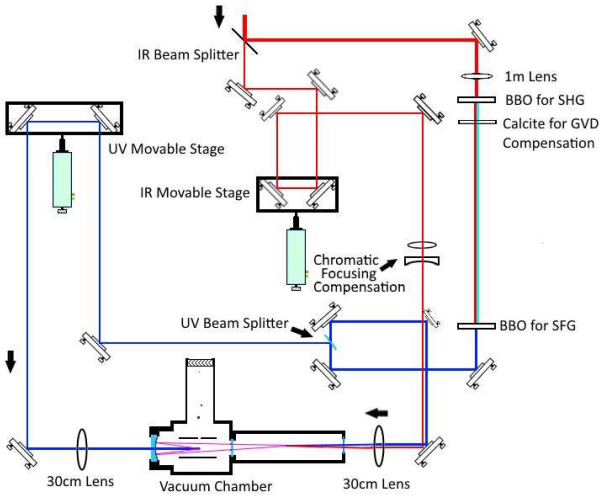

FIG. 1. Schematic diagram of the experimental apparatus. Red, cyan, blue, and purple lines show the fundamental, second harmonic (generated via second harnomic generation (SHG)), third harmonic (UV), and fifth harmonic (VUV) beams respectively. One movable stage is used to temporally overlap the IR and UV pulses for VUV generation, and a second is used to perform the VUV-UV pump-probe experiment.

harmonic (VUV) probe-pulse, ($\lambda = 156$ nm, $\hbar\omega = 7.94$ eV), is generated by focusing the remaining 40 μJ of UV and 100 μJ of residual IR into an Argon gas cell utilizing a non-collinear-four-wave-mixing process[17–19]. This mechanism takes advantage of phase matching at a relatively high pressure (330 Torr) of Argon gas, which increases the conversion efficiency.

The VUV-pulse passes through a 500 μm thick CaF_2 window into an interaction chamber, which is maintained at a pressure of 10^{-7} Torr. The VUV-pulse first passes under the repeller plates of our TOFMS. It is then reflected by a dichroic mirror of radius of curvature $R = 268$ mm. The mirror has a high reflectivity coating of $> 90\%$ at 0° for $156 - 160$ nm light and $< 5\%$ reflectivity for 260 nm and 800 nm. This enables the residual UV and IR radiation left over from VUV generation to be separated from the VUV. The reflected VUV-pulse is then focused under the TOFMS repeller plates. The 5 μJ of UV reserved for the probe is sent through the dichroic mirror and also focused under the TOFMS repeller plates.

The VUV-pump pulse excites the pyrrole molecules to a state about 0.2 eV below the ionization threshold, and the UV probe pulse captures the excited state dynamics by ionizing the molecules at different pump probe delays. The ions generated by the pump and probe pulses are detected with a microchannel plate (MCP) at the end of our TOFMS.

III. COMPUTATIONAL METHODS

In order to interpret the experimental results, we performed electronic structure calculations of the neutral and ionic states of pyrrole. The ground state of pyrrole was optimized using B3LYP/6-31+G(d). The excited state energies and oscillator strengths were calculated using equation of motion coupled cluster for excited states (EOM-EE-CCSD) and the aug-cc-pVTZ basis set. Ionic states were obtained using the equation of motion coupled cluster for ionization potentials (EOM-IP-CCSD) method and the same basis set. The QChem software package was used for these calculations[20]. The NH bond was stretched from its equilibrium position in steps of 0.2 Angstroms, and the excited and ionic states along this coordinate were calculated. The excited states were characterized using natural transition orbitals obtained from the EOM-EE-CCSD method. Molden was used for visualization of the orbitals[21].

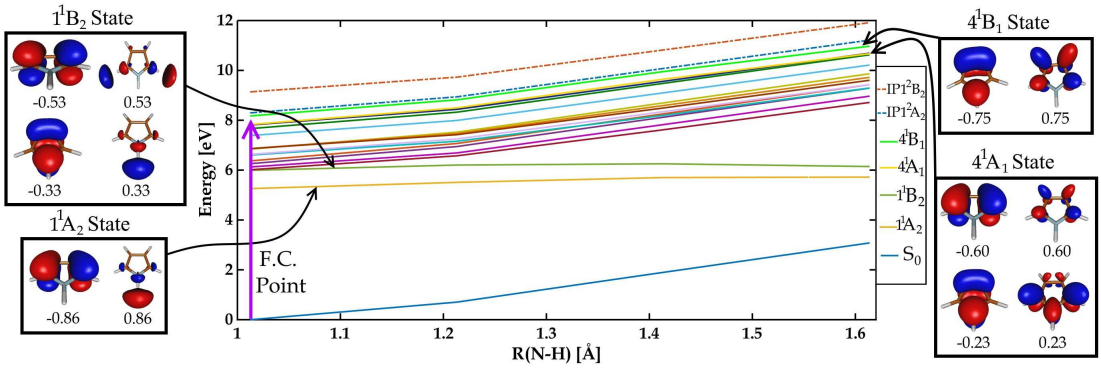

FIG. 2. Natural transition orbitals (left and right sides) and energies as a function of N-H distance (center). The dominant particle-hole pair of orbitals for states 4^1B_1 and 4^1A_1, which are the "bright" states accessible by the VUV-pulse from the ground state, are shown on the right. The singly occupied orbitals for states 1^1B_2 and 1^1A_2, which are the low lying dissociative states along the N-H bond, are shown on the left. The purple arrow indicates the Frank Condon (F.C.) point. The ionic states are shown with dashed lines while the neutral states are shown with solid lines.

Fig.[2] shows the orbitals and the calculated potential energy surfaces along the N-H coordinate. The orbitals

are natural transition orbitals (NTOs) obtained from diagonalizing the transition density[22]. The orbitals are the eigenfunctions of the matrix and represent particle-hole pairs, while the numbers shown in the figure are the eigenvalues. The importance of a particular particle-hole excitation to the overall transition is reflected in the associated eigenvalue. When a state has more than one pair it means that it cannot be described by a single hole-particle representation in the NTO picture. States 4^1B_1 and 4^1A_1 are the high-lying "bright" states that are accessible with the VUV-pump pulse. Looking at their orbitals on the right-hand-side of the plot it is evident that we are driving a $\pi \rightarrow \pi^*$ transition. Orbitals describing states 1^1B_2 and 1^1A_2 are on the left-hand side of the plot and they show that these are $\pi \rightarrow \sigma^*$ states which are not stabilized along the NH coordinate and they can lead to dissociation. The density of states that the VUV-pulse is exciting to is very high, so one would expect very fast radiationless decay from the absorbing state to 1^1B_2 or 1^1A_2. By inspecting the configurations and orbitals describing the 1^1B_2 and 1^1A_2 states and the low lying ionic states we see that ionization is allowed based on Koopmans' theorem. In other words, the two lowest ionic states are described by the same valence orbitals involved in the excited states, and can be accessed by removing the π^* electron. Thus, these excited states can be easily ionized with our probe. In addition to the Koopmans' correlations, the figure makes it clear that for the range of N-H distances considered here, we are energetically able to ionize the molecule from any of the excited states, given their energies relative to the probe photon energy. Thus, the fact that the parent ion signal decays to zero at long time delays indicates that the molecule either relaxes back to the ground state or dissociates.

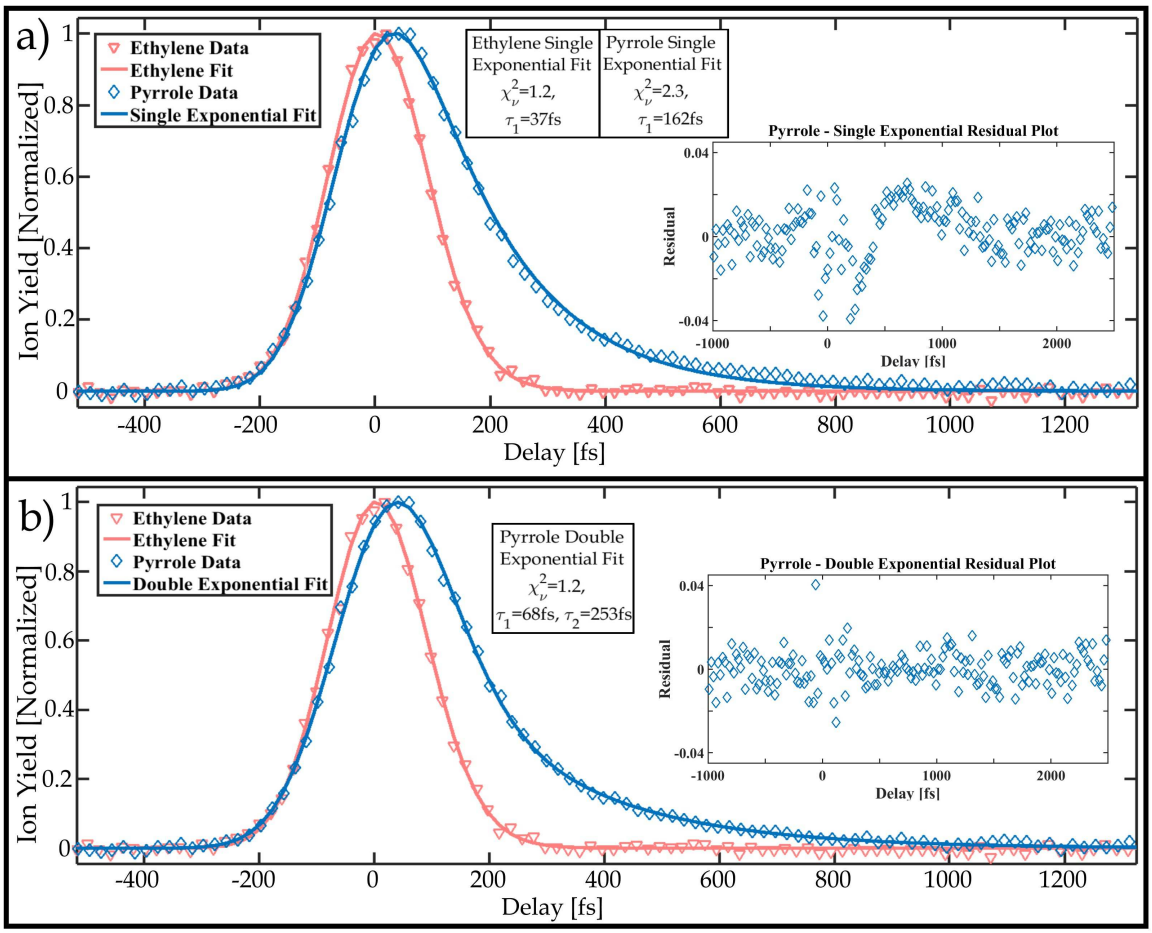

FIG. 3. The red triangle and blue diamond data points show VUV-pump UV-probe measurements performed on ethylene ($C_2H_4^+$) and pyrrole ($C_4H_5N^+$) respectively. The decay constant for ethylene, $\tau = 37$ fs, is extracted with a mono-exponential fit with a $\chi^2 = 1.2$. This decay time is consistent with previous values[23,24]. a) A pyrrole decay constant, $\tau = 162$ fs, is extracted from a mono-exponential fit with a $\chi^2 = 2.3$. The residual plot for this mono-exponential fit to the pyrrole data is shown in the inset. b) Two exponential decay constants, $\tau_1 = 68$ fs and $\tau_2 = 253$ fs, are extracted from a dual-exponential fit with a $\chi^2 = 1.2$. The residuals, shown in the inset plot, are randomly distributed, indicating that this fit is consistent with the measurements.

We note that for larger N-H bond lengths, reference[13] shows the ionization potential from S_1 increasing beyond

our probe photon energy. Thus, our measurements cannot exclude the possibility of dissociation on S_1 despite the lack of fragment ion signal. This point is addressed further below.

IV. RESULTS AND ANALYSIS

As a test and characterization of the apparatus, we recorded the VUV/UV pump-probe signal for ethylene, which has been studied in earlier work and has a very rapid decay[23–25]. These results are shown alongside those for pyrrole in Fig.[3]. The parent ion yield for pyrrole, $C_4H_5N^+$, as a function of VUV/UV pump-probe delay is shown as diamonds. At negative delays the UV-probe pulse comes before the VUV-pump pulse, while for positive delays the VUV pulse comes first. For the simplest fit we assume a mono-exponential decay to describe the molecular dynamics. In order to account for the finite duration of our pump and probe pulses (which have a Gaussian temporal profile), we use a Gaussian convolved with a decaying exponential as our fitting function.

In Fig.[3] the triangles represent VUV-pump UV-probe data for $C_2H_4^+$ from ethylene, and the red curve represents the ethylene data fit to a mono-exponential decay convolved with a Gaussian. The $C_2H_4^+$ data fit yields an exponential decay constant of 37 ± 5 fs with $\chi^2 = 1.2$. Ethylene pump-probe data was collected and refitted for various VUV/UV pulse durations and the resulting spread in the decay constant was used to determine our uncertainty. The VUV excitation of ethylene has been previously studied by Allison[24] and Farmanara[23] where they recorded time constants of $\tau = 21 \pm 4fs$ and $\tau = 40 \pm 20fs$ respectively. Our decay constant being consistent with previously recorded values serves as both a test of our experimental apparatus as well as an indication of where zero time delay is in the pump-probe measurement, since the ethylene decay time is significantly shorter than our pulse duration.

Looking at the fit in panel a of Fig.[3], it is obvious that the mono-exponential pyrrole fit does not describe our data well after 400 fs. The residual plot, Fig.[3] panel a inset, for the pyrrole pump-probe data fit to a mono-exponential clearly has structure, and the fit has a $\chi^2 = 2.3$, indicating that the fit does not accurately reflect the measurement.

Panel b of Fig.[3] shows that a dual exponential function fits the data well with a χ^2 value of 1.2. The decay constants are 68 fs and 253 fs instead of the 162 fs obtained from the mono-exponential fit. Fig.[3] panel b inset is the residual plot for the dual-exponential fit. The residual is randomly distributed, indicating that we have a good fit to our data and that a double exponential decay provides a reasonable description of our measurement.

V. DISCUSSION

A dual-exponential fit implies a two stage process indicating two time-scales for internal conversion, or internal conversion followed by dissociation. In order to determine whether the decay of the parent ion involves dissociation, we monitored the fragment ion yield. The most relevant fragment ion is $C_4H_4N^+$, as dissociation along the N-H coordinate is the most likely to occur[2–4]. Our calculation of the energy levels along the N-H stretching coordinate indicate that the 4.8 eV probe photon energy should be enough to ionize the molecule as it's dissociating along the N-H coordinate. In addition, our calculations of the molecular orbitals for the neutral and cation along the dissociation coordinate indicate that ionization along the dissociation coordinate is not forbidden by Koopman's correlations. However, in the TOFMS we do not see any distinct $C_4H_4N^+$ peak, suggesting that there is no dissociation. In order to allow for the possibility of a small amount of $C_4H_4N^+$ being formed but overwhelmed by the $C_4H_5N^+$ signal in the TOFMS, we binned the lower mass end of the $C_4H_5N^+$ peak with a large enough window so we could capture the $C_4H_4N^+$ peak, if it were there. Fig.[4] shows that any $C_4H_4N^+$ fragment which is formed has the same decay dynamics as the parent ion ($C_4H_5N^+$), indicating the fragment ion is formed after ionization rather than in the neutral. If the molecule were evolving on a dissociative potential after rapid internal conversion, one would expect to see a delayed peak in the fragment dissociation yield.

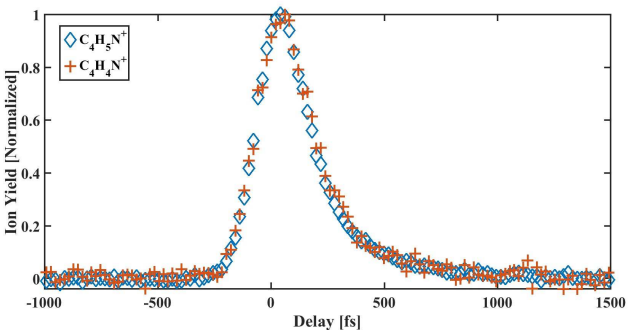

FIG. 4. Pyrrole parent ion $C_4H_5N^+$ and $C_4H_4N^+$ fragment ion yields as a function of pump probe delay.

While our calculation of the energy levels along the N-H stretching coordinate suggest that the 4.8 eV of photon energy should be enough to ionize the $C_4H_4N^+$ fragment as it's dissociating, as an extra precaution we performed pump probe measurements for higher UV pulse energies, such that we could ionize any neutral fragments formed with an ionization potential higher than the UV photon energy via two photon absorption. These measurements yielded the same results, giving further evidence that there is negligible dissociation compared with internal conversion to the ground state.

The fact that the pyrrole measurements cannot be fit-

ted to a single exponential decay while the ethylene data can implies that there is not a single rate limiting step in the case of pyrrole. Given that the relaxation of pyrrole to the ground state starting with an internal energy of 8 eV involves many more states than the relaxation after 5 eV excitation, it is not surprising that there is more than one timescale involved.

VI. CONCLUSION

We make use of a newly developed VUV-pump UV-probe apparatus to study the ultrafast relaxation of highly excited pyrrole. Electronic structure calculations help interpret the measurements, which show a two step decay process with time constants of 68 fs and 253 fs. While earlier measurements that pumped the first absorption band at around 5 eV found a mix of dissociation and internal conversion, we find that the decay of the excited state and our ionization signal is driven largely by rapid internal conversion to the ground state.

VII. ACKNOWLEDGMENTS

We gratefully acknowledge the support from the Department of Energy under Award No. DE-FG02-08ER15984 and Award No. DE-FG02-08ER15983.

[1] D. Blank, S. North, and Y. Lee, Chemical physics **187**, 35 (1994).
[2] J. Wei, J. Riedel, A. Kuczmann, F. Renth, and F. Temps, Faraday discussions **127**, 267 (2004).
[3] J. Wei, A. Kuczmann, J. Riedel, F. Renth, and F. Temps, Physical Chemistry Chemical Physics **5**, 315 (2003).
[4] A. van den Brom, M. Kapelios, T. Kitsopoulos, N. Nahler, B. Cronin, and M. Ashfold, Physical Chemistry Chemical Physics **7**, 892 (2005).
[5] G. Roberts, C. Williams, H. Yu, A. Chatterley, J. Young, S. Ullrich, and V. Stavros, Faraday discussions **163**, 95 (2013).
[6] R. Montero, V. Ovejas, M. Fernández-Fernández, Á. Conde, and A. Longarte, The Journal of chemical physics **141**, 014303 (2014).
[7] V. Vallet, Z. Lan, S. Mahapatra, A. Sobolewski, and W. Domcke, The Journal of chemical physics **123**, 144307 (2005).
[8] G. Roberts, C. Williams, H. Yu, A. Chatterley, J. Young, S. Ullrich, and V. Stavros, Faraday discussions **163**, 95 (2013).
[9] A. Sobolewski, W. Domcke, C. Dedonder-Lardeux, and C. Jouvet, Physical Chemistry Chemical Physics **4**, 1093 (2002).
[10] M. Barbatti, J. Pittner, M. Pederzoli, U. Werner, R. Mitrić, V. Bonačić-Koutecký, and H. Lischka, Chemical Physics **375**, 26 (2010).
[11] K. Saita, M. Nix, and D. Shalashilin, Physical Chemistry Chemical Physics **15**, 16227 (2013).
[12] G. Wu, S. Neville, O. Schalk, T. Sekikawa, M. Ashfold, G. Worth, and A. Stolow, The Journal of chemical physics **142**, 074302 (2015).
[13] M. Barbatti and K. Sen, International Journal of Quantum Chemistry **116**, 762 (2016), ISSN 1097-461X.
[14] M. Vazdar, M. Eckert-Maksić, M. Barbatti, and H. Lischka, Molecular Physics **107**, 845 (2009).
[15] M. Sapunar, A. Ponzi, S. Chaiwongwattana, M. Mališ, A. Prlj, P. Decleva, and N. Došlić, Physical Chemistry Chemical Physics **17**, 19012 (2015).
[16] M. Assmann, T. Weinacht, and S. Matsika, The Journal of chemical physics **144**, 034301 (2016).
[17] M. Beutler, M. Ghotbi, F. Noack, and I. Hertel, Optics letters **35**, 1491 (2010).
[18] M. Ghotbi, M. Beutler, and F. Noack, Optics letters **35**, 3492 (2010).
[19] A. Börzsönyi, Z. Heiner, M. Kalashnikov, A. Kovács, and K. Osvay, Applied optics **47**, 4856 (2008).
[20] Y. Shao, Z. Gan, E. Epifanovsky, A. Gilbert, M. Wormit, J. Kussmann, A. Lange, A. Behn, J. Deng, X. Feng, et al., Molecular Physics **113**, 184 (2015).
[21] G. Schaftenaar and J. Noordik, J. Comput.-Aided Mol. Design **14**, 123 (2000).
[22] R. Martin, The Journal of chemical physics **118**, 4775 (2003).
[23] P. Farmanara, O. Steinkellner, M. Wick, M. Wittmann, G. Korn, V. Stert, and W. Radloff, The Journal of chemical physics **111**, 6264 (1999).
[24] T. Allison, Ph.D. thesis, UC Berkeley: Physics (2010).
[25] H. Tao, T. Allison, T. Wright, A. Stooke, C. Khurmi, J. Van Tilborg, Y. Liu, R. Falcone, A. Belkacem, and T. Martinez, The Journal of chemical physics **134**, 244306 (2011).

VIII. APPENDIX I: ERROR BARS FOR ETHYLENE PUMP PROBE DATA

In order to determine the error in our decay constant for the ethylene pump probe data we tested how the error of our individual fits compared to systematic errors in the experiment. To check this, we varied the pulse duration of our beams and evaluated how the extracted decay constant of ethylene varied.

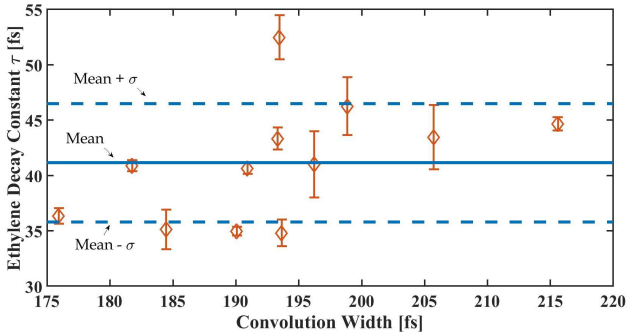

FIG. 5. Decay constant, τ, for fits to ethylene parent ion signal measured with different VUV/UV pulse durations. The error bars on each point are determined by the χ^2 fits. The solid blue line is the mean of the measurements and the dashed blue lines are one standard deviation, σ, above and below the mean.

We moved the grating separation of a pulse compressor in our amplifier to change our pulse durations in our interaction chamber, and reperformed experiments on ethylene at each position. For each grating position we refit our data and from the fit we extracted the FWHM of the convolution of the pump and probe pulse and the decay constant of the molecule. For each individual fit we varied the decay constant, τ, and re-minimized the fitting parameters and determined at what values of τ did χ^2 change by one, and used this as our individual data point error bar.

Fig. 5 shows the results of this compressor scan. It is evident that the spread in the data points is significantly larger than the individual error bars. The individual error bars from the fit vary from $\approx \pm 1$ to ± 2 fs, whereas the standard deviation in all the data points is ± 5 fs, which we take as a more realistic indication of our uncertainty. We note the distribution of decay constants about the mean is not completely random, but shows a slight trend with pulse or cross correlation duration. This indicates that our measurement of the decay time for ethylene might be a slight overestimate based on our pulse duration, which is larger than the measured decay time.

IX. APPENDIX II: KINETIC MODELS

The pump probe data for pyrrole shows a clear dual exponential nature. In order to develop a physical interpretation of this double exponential decay, we consider several kinetic models. These models are shown in Fig. 6. In these models, k is the decay constant between two states and correspond to $1/\tau$ values in the text.

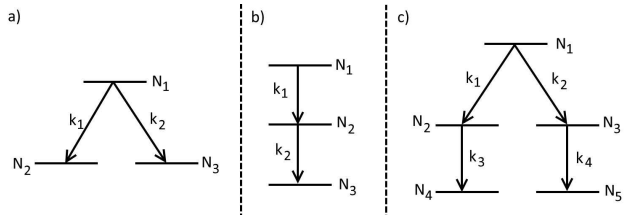

FIG. 6. Different Decay Schemes

In Fig. 6 a) we have the simplest scheme that has two different decays channels from the same state. The population in N_1 can be ionized by the probe to produce the parent ion. The total ionization yield is proportional to the population in N_1, which is

$$N_1 = N_1(0)e^{-(k_1+k_2)t}. \tag{1}$$

In this model $N_1(0)$ is the initial population in N_1. This model yields a single exponential, hence it cannot explain the double exponential nature of our pyrrole data.

We then consider Fig. 6 b). Here we have an effective three level model for the dynamics, where decay from the initial excited state to an intermediate state gives one timescale, while decay of this intermediate state to the ground state gives the second. Both the initial excited state and intermediate state can be ionized by the probe pulse to produce the parent ion. In this simple picture, the total ionization yield is proportional to the sum of the populations, N, in the intermediate and initial states, N_1 and N_2, with

$$N = N_1(0)\left[1 + \frac{k_1}{k_2 - k_1}\right]e^{-k_1 t} - \frac{k_1}{k_2 - k_1}N_1(0)e^{-k_2 t}. \tag{2}$$

This model would seem to explain the fit to a double exponential with two distinct decay constants. But, when we constrain our fit to Eq. (2), and the amplitudes are not allowed to evolve freely, the fit cannot capture the dynamics.

Finally, we consider Fig. 6 c) where we have two parallel decays (5 levels system). Here we consider that the initial excited state, N_1, can decay via two channels, N_2 and N_3. From N_2 the system decays into N_4 and from N_3 the system decays into N_5. Again, we assume the total ionization yield is proportional to the sum of the populations, N, in the intermediate and initial states N_1, N_2,

and N_3. In this model, the combined signal, N, is

$$N = \left[N_1(0) + \frac{N_1(0)k_1}{k_3 - k_1 - k_2} + \frac{N_1(0)k_2}{k_4 - k_1 - k_2}\right] e^{-(k_1+k_2)t} - \frac{N_1(0)k_1}{k_3 - k_1 - k_2} e^{-k_3 t} - \frac{N_1(0)k_2}{k_4 - k_1 - k_2} e^{-k_4 t}. \quad (3)$$

This model, even with the constrained amplitudes, fits our data very well. This model gives values $\tau_1 = 293$ fs, $\tau_2 = 84$ fs, $\tau_3 = 290$ fs, and $\tau_4 = 70$ fs with a χ^2_ν of 1.26.

While this model fits our data well, the real dynamics are undoubtedly much more complicated. These kinetic models show that the double exponential nature we see in the pyrrole data cannot be accurately described by the simple pictures seen in Fig. 6 a) and b). This is not surprising, considering the complexity of pyrrole's relaxation dynamics with many states involved.